



CrossMark
click for updates

Cite this: *RSC Adv.*, 2014, 4, 32866

Synthesis and characterization of perylene diimide based molecular multilayers using CuAAC: towards panchromatic assemblies†

Evan E. Beauvilliers, Michael R. Topka and Peter H. Dinolfo*

Three perylene diimides (PDI) were synthesized with propargyl groups at the diimide positions to enable the fabrication of molecular multilayer thin films *via* sequential copper(I) catalyzed azide-alkyne cycloaddition (CuAAC) coupling reactions in a layer-by-layer (LbL) fashion. The new PDIs with phenoxy (PhO-PDI), dodecylthiol (Thiol-PDI), and pyrrolidine (Pyrr-PDI) substituents in bay positions have optical absorption spectra that span a large portion of the visible region. Multilayer growth on 11-azidoundecylsiloxane coated silica glass and indium tin oxide (ITO) surfaces was demonstrated up to 10 bilayers of each PDI with 1,3,5-tris(azidomethyl)-benzene (**N₃Mest**) *via* optical and infrared spectroscopy. Polarized UV-visible absorption measurements showed a strong dependence on the orientation of the film in the light path and was consistent with a preferential orientation of the PDI molecules in the film at 40–42° with respect to the substrate surface. Grazing-angle attenuated total reflectance (GATR) infrared spectra of the films show an increase in content of unreacted azides during multilayer growth from **N₃Mest** as a result of the smaller molecular footprint as compared to the PDI components. Electrochemical scans of the multilayer films grown on ITO exhibited reversible two-electron reduction waves for the PDIs with linear increases in charge with bilayer growth. The electrochemically derived surface coverages of PDIs averaged 1.2–1.3 × 10¹⁴ molecules per cm² for each layer added to the multilayer films. The flexibility of the CuAAC based LbL assembly methodology is highlighted by the assembly of a mixed multilayer film containing five layers of each PDI, resulting in a panchromatic film that is a summation of individual chromophores.

Received 13th May 2014
Accepted 17th July 2014

DOI: 10.1039/c4ra04512b

www.rsc.org/advances

Introduction

Research into the use of molecular components for photovoltaic and artificial photosynthetic devices has been on-going for several decades. A common approach to designing such devices mimics natural photosynthetic systems by coupling discrete systems to handle the various photo- and electrochemical processes of light absorption, energy transfer, charge separation, and chemical catalysis.^{1–3} Electrode or semiconductor (SC) interfaces are often exploited in molecular-based systems to help facilitate a number of these reactions. The electrode can play several important roles; from facilitating charge transfer and collection, to the physical separation of half-cell reactions, among others. Thus, developing adaptable methods to chemically modify the electrode surface with hierarchical molecular structures and understanding the charge-transfer and photo-physical processes occurring amongst the molecular

constituents is of central importance to the field of artificial photosynthesis.

There have been numerous examples of molecular donor-acceptor arrays created to study both energy- (EnT) and electron-transfer (ET) for application in photovoltaic and artificial photosynthetic systems.^{4–9} The development of large, extended donor-acceptor systems consisting of more than two chromophores have been reported, but are generally more difficult to synthesize and anchor to electrode interfaces. Nevertheless, such multi-component systems would be beneficial in the design of Light Harvesting Arrays (LHA) that mimic natural photosynthetic systems enabling broadband light absorption. Unfortunately, the synthetic complexity of many of these arrays may make it difficult and time consuming to study the photoelectrochemical properties of a range of light harvesting assemblies on electrode surfaces. Thus, we have chosen to utilize molecular layer-by-layer (LbL) assembly techniques to facilitate the fabrication of chromophoric arrays on surfaces.

The LbL fabrication process is a bottom-up approach to surface functionalization that allows for the straightforward modification of a substrate in a highly tuneable fashion. The process relies upon the use of self-limiting reactions at a substrate surface that restrict film formation to a single

Department of Chemistry and Chemical Biology, Rensselaer Polytechnic Institute, 110 Eighth Street, Troy, New York 12180, USA. E-mail: dinolp@rpi.edu; Fax: +1-518-276-4887; Tel: +1-518-276-2326

† Electronic supplementary information (ESI) available: UV-visible absorption, IR spectra, and CVs. See DOI: 10.1039/c4ra04512b

monolayer at each step. The primary advantage of this technique is that single monolayer formation can be achieved by simply immersing the sample in solutions of the various components sequentially, thus avoiding lengthy and tedious purification steps associated with traditional synthesis. Complex molecular structures, such as multicomponent LHAs described above, are often difficult to organize from homogeneous materials in solution and are best obtained through the “bottom-up” synthetic approach inherent to LbL techniques. LbL formation of molecular materials on surfaces has been achieved by a number of different interlayer coupling methods, including siloxanes,^{10–16} zirconium phosphonates,^{17–22} imides,²³ and transition metal coordination chemistry.^{24–29}

We have recently developed a molecular multilayer assembly technique utilizing copper(i) catalyzed azide–alkyne cycloaddition (CuAAC) chemistry as both a means of linking molecular layers together and anchoring the films to electrode and oxide surfaces.^{30–34} This LbL fabrication technique provides a means to generate ordered, reproducible, and uniform films that are relatively straightforward to synthesize. Our initial studies in this area have focused on multilayers films comprised primarily of tetra-phenylporphyrin chromophores, but we ultimately would like to expand upon the number of ethynyl-functionalized chromophores available to achieve broadband light absorption *via* a synthetic LHA comprised of multiple dyes. Perylene-3,4,9,10-tetracarboxydiimides (PDIs) have received significant attention as building blocks in synthetic LHA.^{35–37} They are optically and thermally stable and can be readily functionalized to tune their reactivity and optical properties.³⁸ This tunability allows the development of PDIs that absorb across the visible spectrum and can participate in CuAAC reactions to produce multilayer thin films. Furthermore, they are known to be capable of efficient Förster resonance energy transfer (FRET) and therefore offer intriguing possibilities for light harvesting arrays.³⁹ In our initial work describing the development of the CuAAC based molecular LbL scheme, we utilized a phenoxy substituted PDI with *p*-ethynylaniline at each of the diimides for multilayer growth. Unfortunately, the synthesis of this PDI involved seven sequential steps starting from perylene-3,4,9,10-tetracarboxylic dianhydride (PTCDA).³⁰ Herein we describe the synthesis of three different PDIs with propargyl amines at each of the diimides and have absorption bands which span the visible spectra. Utilization of propargyl amine allowed for a shorter synthetic procedure and higher yields. Multilayer growth *via* the CuAAC LbL method was followed and characterized by electronic absorption spectroscopy, grazing angle attenuated total reflectance IR and surface electrochemistry.

Results and discussion

Perylene diimide synthesis

Scheme 1 contains the three perylene diimides (PDIs) surveyed in this study. Each chromophore is based on a di-bromo PDI that has been substituted in the bay positions of the perylene core with *p*-(*t*-butyl)phenol (**PhO-PDI**), dodecanethiol (**Thiol-PDI**) and pyrrolidine (**Pyrr-PDI**). Substitution of the bay

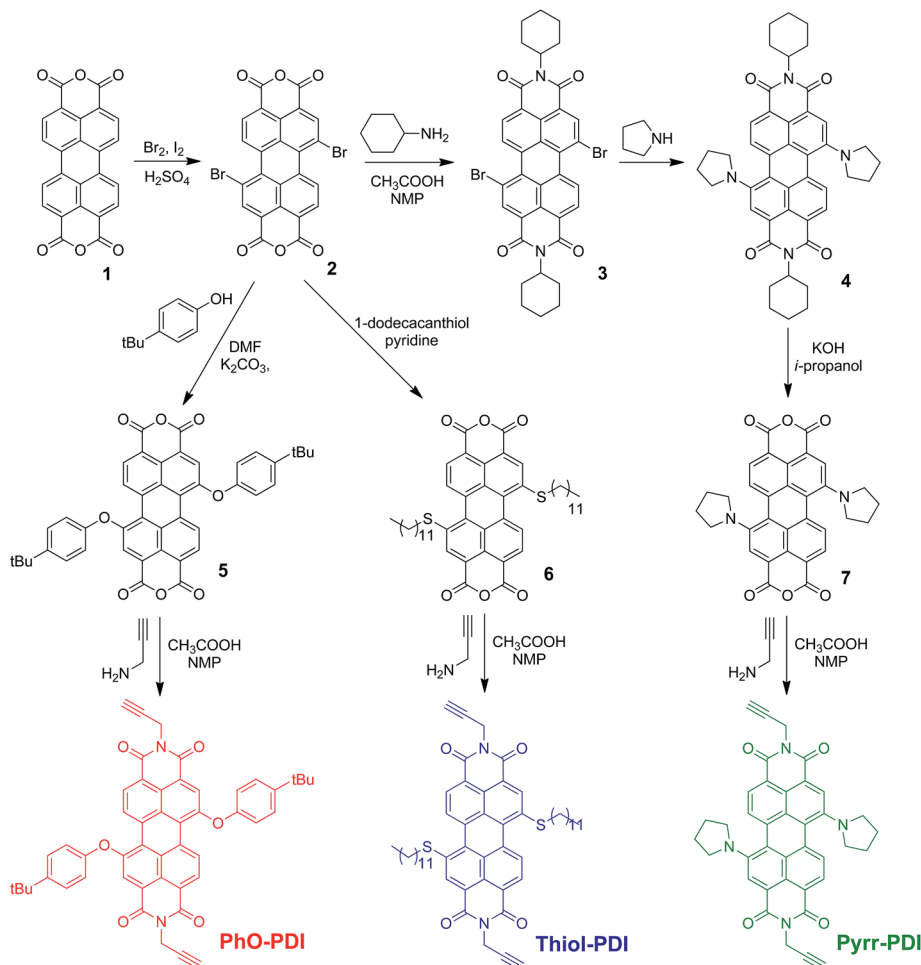
positions of PDIs with π -donors or acceptors affect the HOMO and LUMO energy levels and thus have a significant effect on the photophysical and electrochemical properties, along with enhanced solubility.⁴⁰ On the other hand, substituents on the diimide N atoms show relatively small effects on orbital energies, but generally play a significant role in controlling the solubility of the PDIs. The synthetic methodology for the three PDIs is outlined in Scheme 1. All synthetic details and characterizations are included in the supporting information.

Previous reports in literature typically employ a diimide protection and subsequent deprotection step before and after the nucleophilic substitution of the perylene bay positions.⁴¹ In this synthetic scheme, we were able to circumvent these protection-deprotection steps for **PhO-PDI** and **Thiol-PDI** by direct modification of di-Br-PTCDA (**2**) with *t*-butylphenol and 1-dodecanethiol respectively. Addition of propargyl amine to the di-PhO-PTCDA (**5**) and di-thiol-PTCDA (**6**) in NMP with a catalytic amount of acetic acid gave **PhO-PDI** and **Thiol-PDI**. Unfortunately, reaction of **2** with pyrrolidine gave a mixture of products, of which di-Pyrr-PTCDA (**7**) could not be extracted in reasonable yield. Thus, we utilized cyclohexylamine as a protecting group for the dianhydrides prior to functionalization with pyrrolidine (**4**). Deprotection with KOH in isopropanol gave **7** which was then reacted with propargyl amine to give **Pyrr-PDI**. Even with the additional protection steps, the overall synthesis of **Pyrr-PDI** was slightly shorter than our previous *p*-ethynylaniline functionalized PDI.³⁰

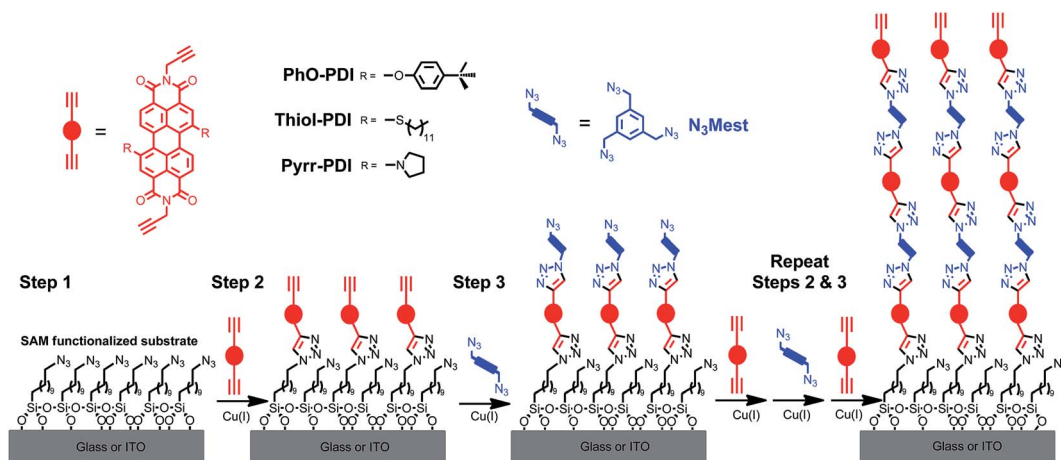
Multilayer growth

Molecular multilayer growth utilizing **PhO-PDI**, **Thiol-PDI**, and **Pyrr-PDI** was accomplished using the CuAAC-based LbL assembly technique previously described by our laboratory.^{30–34} Scheme 2 outlines the multilayer fabrication methodology. The process starts with the functionalization of glass or indium tin oxide (ITO) electrodes with an azido terminated alkyl siloxane self-assembled monolayer. The LbL technique utilizes two sequential self-limiting surface CuAAC reactions of the di-ethynyl PDIs and a multi-azido linker, 1,3,5-tris(azidomethyl) benzene (**N₃Mest**), for growing molecular layers on a functionalized substrate. Each sequential coupling reaction generates alternating alkyne or azide functionality to the surface (Scheme 2, steps 2 & 3). From here on, we describe a single bilayer as consisting of one di-ethynyl-PDI layer and one azido-linker layer. Because of the selectivity and high yield of the CuAAC reaction, the versatility of this technique allows for relatively easy introduction of various dyes in a controlled fashion.

To follow multilayer growth, UV-vis spectroscopy and IR spectroscopy were employed to monitor the assembly of dyes on various transparent oxide surfaces. Fig. 1 shows the absorption spectra during the addition of ten bilayers of each PDI and **N₃Mest** on ITO coated glass slides. Experimental conditions for the surface CuAAC reactions are included in the Experimental section. Each PDI displays linear absorption increases through the addition of ten bilayers (Fig. 1 and S1†). The use of a tris-azido linker (**N₃Mest**) is thought to be important to the overall efficiency of the CuAAC-based LbL



Scheme 1 Synthetic route for the preparation of PhO-PDI, Thiol-PDI and Pyrri-PDI.



Scheme 2 CuAAC-based LbL assembly scheme.

assembly. If either the PDI or azido-linker additions fail to react quantitatively, then there would be a decrease in absorbance in the subsequent bilayer. However, the tri-azido functionality of N_3Mest provides a dendritic healing effect that

ensures a high density of surface azides for the following bis-ethynyl dye. This approach allows for consistent linear multi-layer growth over tens of bilayers.⁴²

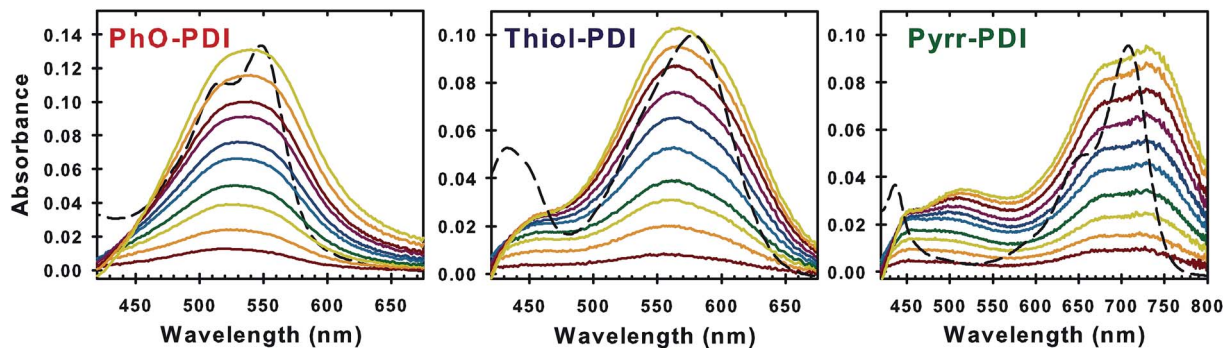


Fig. 1 Visible region absorption profiles obtained during the growth of ten bilayers of PhO-PDI (left), Thiol-PDI (middle), and Pyrr-PDI (right) on ITO (solid colored lines) with N_2 Mest. (The sharp decrease in absorption at 430 nm is due to background subtraction of the ITO substrate.) The dashed black lines represent the absorption spectra of the PDIs in chloroform.

Multilayer electronic absorbance analysis

The normalized absorbance profiles of PhO-PDI, Thiol-PDI, and Pyrr-PDI in chloroform solutions are included in Fig. 1 (dashed black lines). The absorption spectra for all three PDI-based multilayer films contain features that resemble the chromophores in solution, but are noticeably broader. This effect is consistent with aggregation occurring within the film which is a common phenomenon for PDIs due to the strong intermolecular π - π interaction of the planar perylene core.^{6,43–51} Multilayer films comprised of PhO-PDI and Pyrr-PDI, display a change in absorption ratio between the major vibronic molecular absorptions, I_A^{0-1} vs. I_A^{0-0} , from the $S_0 \rightarrow S_1$ transition. An increase in the I_A^{0-1}/I_A^{0-0} ratio is predicted and experimentally observed for H-type aggregates between PDI chromophores. The multilayer spectra for Thiol-PDI also show an increase in absorption intensity on the high energy side of the band, but the lack of clear vibronic transitions makes this aggregation effect less apparent than PhO-PDI and Pyrr-PDI. The increased broadness and lack of vibronic detail in the multilayer spectra indicates that a range of aggregate forms are present in the film. This is in contrast to our previous studies using a phenoxy substituted PDI with *p*-ethynylaniline at each of the diimides that showed clear vibronic bands with a significant increase in the I_A^{0-1}/I_A^{0-0} ratio. The flexible propargyl functionality of PhO-PDI, Thiol-PDI, and Pyrr-PDI likely allows for greater range of aggregate forms in the multilayer, resulting in the broadened spectra.

Polarized absorption spectra were obtained for the multilayers to elucidate the presence of molecular structure within the films. Absorption spectra were taken with polarized light oriented every 30° from 0° to 180° for 10 bilayers of each PDI with the slide held at 90° , 60° and 45° relative to the incident light path. Fig. 2 shows plots of the absorbance at the absorption maximum for the PhO-PDI as a function of polarization angle and the angle between the slide and the incoming polarized light. A similar trend was found for Thiol-PDI and Pyrr-PDI (Fig. S2†). In all three multilayer films, there was a minimum absorbance at horizontally polarized light (90°) and a maximum absorbance with vertically polarized light (0° and 180°) when the slide was held at a 60° and 45° angle to the incoming light (Fig. 2, green squares and red triangles). In

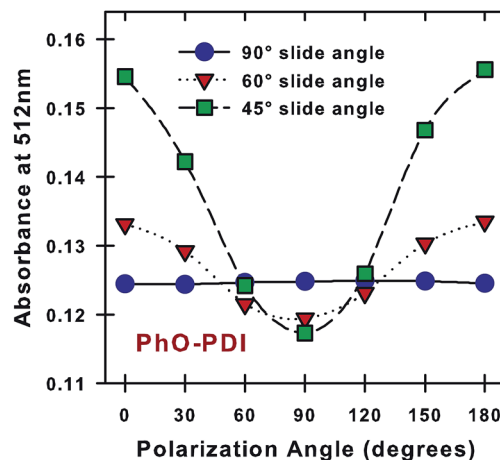


Fig. 2 The peak absorbance of PhO-PDI at 520 nm as a function of polarization angle of the incident light and the angle of the slide with respect to the incident light path.

contrast, when the slide was held normal to the incoming polarized light, there was no polarization dependence (Fig. 2, blue circles). The dichroic ratio ($D(\lambda)$) of the absorbance for the horizontal (A_h) and vertically (A_v) polarized light can be described by

$$D(\lambda) = \frac{A_h}{A_v} = \frac{2 \sin^2 \alpha \sin^2 \gamma}{2 - \sin^2 \gamma} + \cos^2 \alpha$$

where α is the angle of the sample relative to the incident light path and γ is the angle of the transition dipole moment relative to the substrate surface.^{52–54} Since the $S_0 \rightarrow S_1$ transition for PDIs are primarily $\pi \rightarrow \pi^*$ in nature with the electronic transition dipole moment oriented along the long axis of the molecule (imide N-N),⁵⁵ γ also reports on the orientation of the PDI molecules in the film relative to the substrate surface. For 10 bilayers of PhO-PDI, Thiol-PDI, and Pyrr-PDI grown on glass, γ was found to be 40° , 42° , and 40° respectively. The higher dichroic ratio of the absorption spectra with the sample slide held at a 45° relative to the incident light path over that of 60° is consistent with a preferential orientation of the PDI molecules grown upright with respect to the substrate surface.

Cooperatively, the lack of polarization dependence with the slides held normal (90°) to the incoming light path indicates the PDI molecules are randomly oriented in the plane of the slide.

Infrared analysis

Fig. 3 shows a selection of Grazing-angle attenuated total reflectance (GATR) FTIR spectra obtained at each step in the multilayer growth up to 10 bilayers of **Pyrr-PDI** with **N₃Mest** on an ITO electrode. (GATR-FTIR spectra for multilayer growth with **PhO-PDI** and **Thiol-PDI** with **N₃Mest** are shown in Fig. S3†). The initial azido-SAM functionalized ITO glass substrate (layer 0.5) shows a band at $2,100\text{ cm}^{-1}$ that is expected for a terminal alkyl azide.^{56,57} Other stretches at $2,950\text{ cm}^{-1}$ and $2,860\text{ cm}^{-1}$ are the typical CH stretches for alkyl siloxane SAMs anchored onto an oxide surface.^{58,59} After performing the CuAAC reaction to attach the bis-ethynyl **Pyrr-PDI**, the azide absorption almost completely disappears and several new IR absorptions appear (Fig. 3, layer 1) including strong stretches at 1700 and 1660 cm^{-1} which are typical of the diimide groups in PDIs.^{60,61} The decrease of the azide stretch is consistent with the reaction with the ethynyl group en route to forming the triazole *via* CuAAC. Assigning the triazole CH stretch in the dense IR region containing various aromatic CH stretch frequencies was not possible due to its weak intensity. The IR spectrum after addition of the **N₃Mest** linker layer to the film reveals the regeneration of the azide stretch at 2100 cm^{-1} , which indicates successful replenishment of azides on the surface has been achieved (Fig. 3, layer 1.5).

Because the penetration depth of IR light in the GATR technique is typically $0.5\text{--}1\text{ }\mu\text{m}$ for organic films, the spectra are representative of the entire nanoscale multilayer composition.⁶² Therefore, this technique can also be used to track multilayer growth. Fig. 4 shows the integrated carbonyl (C=O) stretches at 1700 and 1660 cm^{-1} and azide at 2100 cm^{-1} as a function of layer. (Half-integer layers are azide terminated (azido-SAM or **N₃Mest**) and full integer layers are following a reaction with

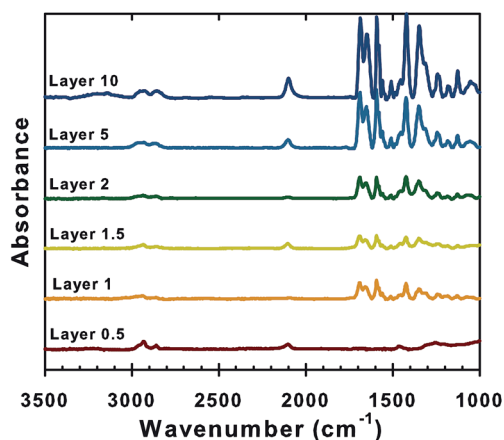


Fig. 3 Selection of GATR-FTIR spectra collected during the assembly of 10 bilayers of **Pyrr-PDI** and **N₃Mest** on ITO. Half-integer layers are azide terminated (azido-SAM or **N₃Mest**) and full integer layers are following a reaction with **Pyrr-PDI**.

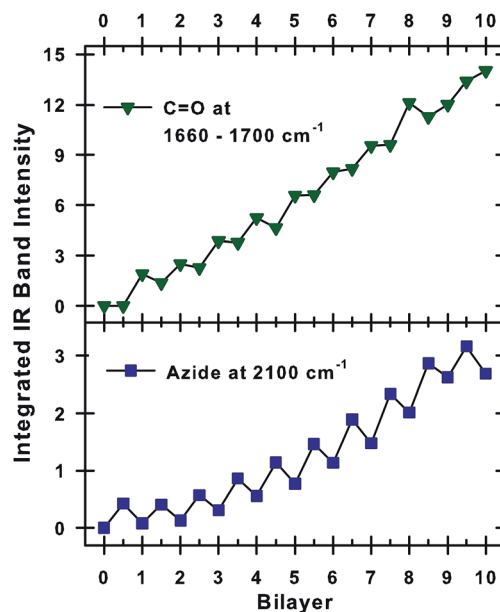


Fig. 4 The integrated IR absorbance intensity the two carbonyl vibrational modes at 1700 cm^{-1} and 1660 cm^{-1} (top) and azide vibrational mode at 2100 cm^{-1} (bottom) as function of layer addition with **Pyrr-PDI** and **N₃Mest** on ITO. Half-integer layers are azide terminated (azido-SAM or **N₃Mest**) and full integer layers are following a reaction with **Pyrr-PDI**.

Pyrr-PDI.) As expected, the C=O stretches of **Pyrr-PDI** increase in absorbance with sequential additions and remain constant with addition of **N₃Mest** linker layers. The azide mode shows an oscillating trend, increasing at each **N₃Mest** linker layer and decreasing upon addition of **Pyrr-PDI**. (The greater variation in C=O stretching intensity *vs.* the azide is due to imperfect background subtraction in the region below 1700 cm^{-1} .) The overall increasing trend of the 2100 cm^{-1} stretch is consistent with the presence of unreacted azides in the multilayer film from the tri-functional **N₃Mest** linker. Similar trends were observed with this azido linker during multilayer growth with tetraphenylporphyrins.⁴² Similar trends in azide and diimide C=O were also observed with **PhO-PDI** and **Thiol-PDI** (Fig. S4†).

Multilayer electrochemistry

Cyclic voltammetric (CV) scans were performed on the PDI multilayer films assembled on ITO electrodes to examine their electrochemical properties. PDI's with bay substitutions of phenol, thiol, and pyrrolidine typically show two reversible single electron reductions associated with each diimide group.^{38,63,64} Fig. 5 demonstrates the typical electrochemical behavior of the multilayer films of **PhO-PDI**, **Thiol-PDI**, and **Pyrr-PDI**, from one through five bilayers each. The CVs for all PDI based multilayer films displayed a linear relationship between peak current and scan rate consistent with a surface bound species.⁶⁵ Each of the PDI multilayers display two chemically reversible electron reductions, however the moderate peak splitting indicates the electron transfer rate is somewhat limiting at a scan rate of 1 V s^{-1} . In addition to

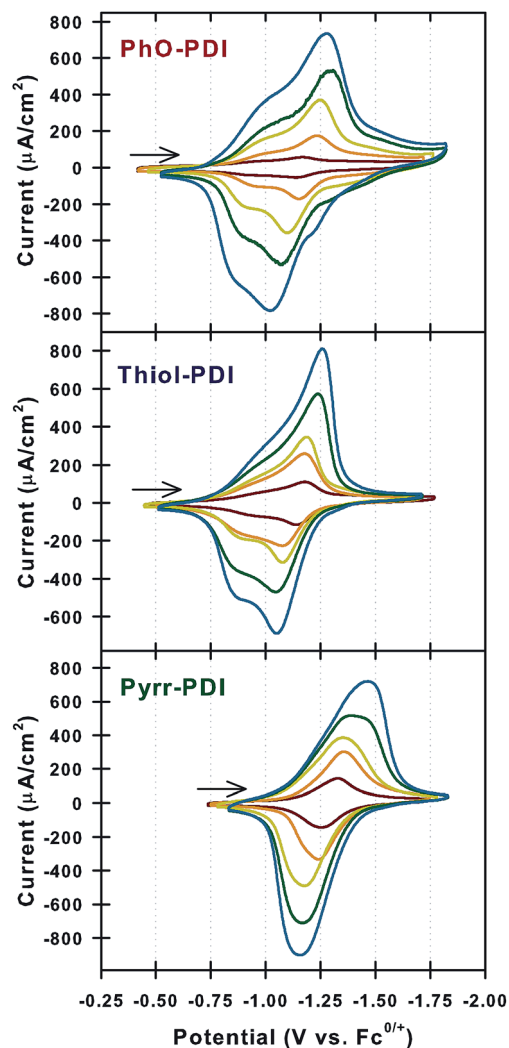


Fig. 5 Cyclic voltammograms of one through five bilayers of PhO-PDI (top), Thiol-PDI (middle) and Pyrr-PDI (bottom) assembled on an ITO electrode. CVs were obtained at scan rate of 1 V s^{-1} with 0.1 M TBAP in anhydrous acetonitrile as the electrolyte. The arrow shows the initial scan direction.

reductions, pyrrolidine substituted PDIs are also known to exhibit two reversible oxidations.⁶⁴ Fig. S5[†] contains CVs of **Pyrr-PDI** taken over a large potential window showing both two electron oxidation and reduction waves. As can be seen in Fig. 5 and S6,[†] the peak current and charge for the reductive waves of each PDI increase with additional layers added to the multilayer film. This trend mirrors the absorption increases during film growth and is consistent with complete electrochemical reduction of the multilayer assemblies. Integration of the CVs provides the charge density (σ) and effective (electrochemically active) molecular surface coverage (Γ_{eff}) of the film (Table 1). There is some variability in the electrochemically derived Γ_{eff} vs. the number of layers added to the film as compared to the highly linear absorbance growth profiles. We observed that the first few layers are somewhat unstable under electrochemical conditions and degrade slightly after a few cycles. The thicker multilayer films, on the other hand, are more stable upon

Table 1 Electrochemical data: charge density (σ), and effective surface coverage (Γ_{eff}) of the multilayer thin films

Multilayer components	Number of bilayers	σ ($\mu\text{C cm}^{-2}$)	Γ_{eff} (molecules cm^{-2})
PhO-PDI and N_3Mest	1	23	0.7×10^{14}
	2	54	1.7×10^{14}
	3	120	3.7×10^{14}
	4	176	5.5×10^{14}
	5	229	7.1×10^{14}
Thiol-PDI and N_3Mest	1	37	1.2×10^{14}
	2	73	2.3×10^{14}
	3	95	3.0×10^{14}
	4	159	5.0×10^{14}
	5	224	7.0×10^{14}
Pyrr-PDI and N_3Mest	1	32	1.0×10^{14}
	2	75	2.3×10^{14}
	3	117	3.6×10^{14}
	4	173	5.4×10^{14}
	5	235	7.3×10^{14}

repeated electrochemical cycles and thus may be more representative of the effective electroactive molecular surface coverage.

Panchromatic multilayer assemblies

The versatility of the CuAAC based LbL methodology allows for complete control over the molecular architecture of thin films

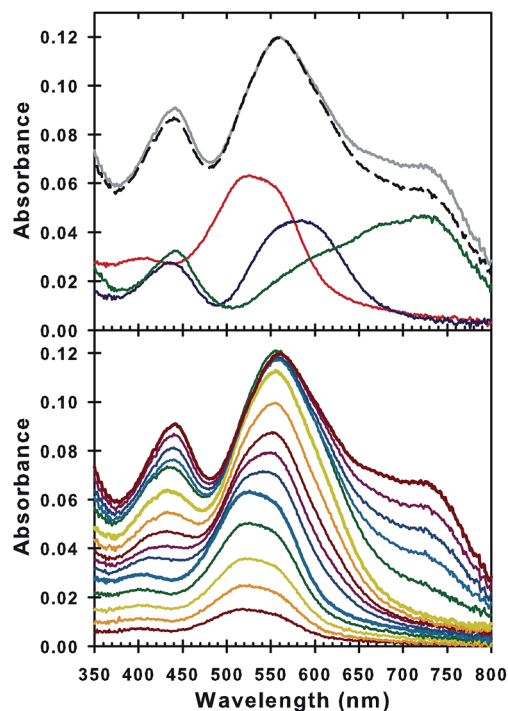


Fig. 6 Bottom: Visible absorption profiles obtained during the growth of a mixed multilayer comprised of five bilayers of each PDI on glass. Top: Final absorption profile of the fifteen bilayer film (gray line) and absorption spectra for five bilayers of each component on glass. The sum of the individual component films, shown as the dashed black line, is nearly identical to the mixed multilayer.

making this feature especially desirable for designing broadband light harvesting assemblies based on molecular components. Fig. 6 demonstrates the interchangeability of these dyes for multilayer growth on an oxide surface. First, five bilayers of **PhO-PDI** were grown on the SAM-functionalized glass, then five layers **Thiol-PDI** and finally five layers of **Pyrr-PDI**. The combination of all three perylene dyes yields a film that absorbs throughout the visible region. Each PDI shows a linear increase in absorbance during the mixed multilayer growth (Fig. S7†). The resulting film comprised of five layers of each PDI shows an absorption spectrum that is a simple summation of the individual components (Fig. 6 top).

Conclusion

Three new di-propargyl functionalized PDIs were synthesized to enable the fabrication of multilayer thin films utilizing CuAAC chemistry. The new PDIs with phenoxy (**PhO-PDI**), dodecylthiol (**Thiol-PDI**), and pyrrolidine (**Pyrr-PDI**) substituents in bay positions have optical absorbance spectra that span the visible region. Multilayer growth on glass and ITO substrates was achieved with each PDI *via* the CuAAC method to yield films up to fifteen bilayers thick with linear growth profiles. These films were analyzed by polarized electronic absorption, GATR-IR, and electrochemistry. Polarized UV-visible absorption measurements showed a strong dependence on the orientation of the film in the light path, consistent with a preferential orientation of the PDI molecules in the film. IR spectra of the films were consistent with the CuAAC reaction between layers and surface attachment of the PDI components. Electrochemical scans of the multilayer films grown on ITO showed reversible reductions of the PDIs and linear charge densities up to five bilayers.

The selectivity of the CuAAC reaction towards azides and alkyne groups provides great flexibility with this multilayer growth method by allowing a wide range of molecular components to be used for film assembly. Thus, this methodology allows for complete tunability in the multilayer optical and electrochemical properties. The ability to easily incorporate different dyes into multilayer assemblies has the potential to develop efficient light harvesting materials for dye-sensitized solar cells or other artificial photosynthetic devices.

Experimental section

General methods

NMR spectra were obtained on a Varian 500 MHz spectrometer and chemical shifts were referenced to that of the solvent. LR MALDI-TOF MS were obtained on a Bruker Ultraflex III. HR ESI MS were obtained on a Thermo Electron Finnigan TSQ Quantum Ultra.

Materials

Solvents, ACS grade or better, were purchased from Sigma Aldrich or Fischer Scientific and used as received unless specified. Toluene was purged with nitrogen and dried over 4 Å molecular sieves before use. Acetonitrile for electrochemistry

was dried by recirculating the nitrogen purged solvent through a solid-state column purification system (Vacuum Atmospheres Company, Hawthorne, CA) prior to use. Sodium ascorbate (Aldrich) and tetrabutylammonium hexafluorophosphate (TBAP, Acros) were used as received. 11-azidoundecyltrimethoxysilane, 1,3,5-tris(azidomethyl)-benzene (**N₃Mest**), tris-(benzyltriazolylmethyl)amine (**TBTA**), and 1,3,5-tris-(hydroxypropyltriazolyl)amine (**THPTA**) were available from previous studies or were synthesized according to literature methods.^{66–70} Glass slides were purchased from SPI Supplies. ITO-coated glass slides were purchased from Delta Technologies (polished float glass, ITO coated one surface, $R_s = 4–8 \Omega$). **2**,^{41,71} **3**,^{41,71} **4**,⁷² **5**,⁷³ and **7** (ref. 41) were synthesized according to published procedures. The preparation of **2** (**Br₂-PTCDA**) generates a mixture of both the 1,7- and 1,6-isomers in a 9 : 1 ratio based on ¹H NMR. These isomers could not be efficiently separated and were carried throughout the synthetic scheme.⁴¹

Synthetic procedures

Synthesis of 1,7-di(dodecylthio)perylene-3,4:9,10-tetracarboxylic acid dianhydride (mixture of 1,6- and 1,7-isomers) (6). Following a similar literature method,⁷⁴ **2** (554 mg, 1 mmol), 1-dodecanethiol (600 mg, 3.2 mmol), NaOH (100 mg, 2.5 mmol), and 30 mL of pyridine were added to a reaction flask, purged with N₂ and refluxed for 3.5 h. The mixture was poured into 100 mL of 10% (v/v) HCl and extracted with DCM. The organic solution was collected, dried, and the solvent removed. The purple crude product was purified by chromatography (silica gel, 95/5 DCM/MeOH) resulting in a total mass of 424 mg (53%) of purple product. ¹H NMR (CDCl₃, 1,6-isomer): 8.91 (d, 2H, *J* = 8.0 Hz), 8.83 (d, 2H, *J* = 8.0 Hz), 8.72 (s, 2H), 3.24 (t, 4H, *J* = 7.4 Hz), 1.71 (q, 6H, *J* = 7.4 Hz), 1.45 (q, 4H, *J* = 7.0 Hz), 1.3–1.2 (br, 32H), 0.89 (t, 6H, *J* = 6.7 Hz); ¹H NMR (CDCl₃, 1,7-isomer): 8.94 (d, 2H, *J* = 8.0 Hz), 8.79 (s, 2H), 8.74 (d, 2H, *J* = 8.0 Hz), 3.24 (t, 4H, *J* = 7.3 Hz), 1.71 (q, 4H, *J* = 7.3 Hz), 1.46 (q, 4H, 7.0 Hz), 1.3–1.2 (br, 32H), 0.88 (t, 6H, *J* = 6.7 Hz); HR-ESI MS *m/z* calculated for [M][−] 792.3524 found [M][−] 792.3510.

Synthesis of *N,N'*-dipropargyl-(1,7)-di(4-*tert*-butylphenoxy)perylene-3,4:9,10-bis(dicarboximide) (mixture of 1,6- and 1,7-isomers) (PhO-PDI). 5 (285 mg, 0.41 mmol), propargylamine (71 mg, 1.2 mmol), 0.10 mL of glacial acetic acid, and 20 mL of anhydrous NMP were added to a reaction flask. The reaction mixture was stirred at 80 °C under N₂ for 12 hours. The reaction mixture was cooled to room temperature and 100 mL of 10% (v/v) aqueous HCl was added to the solution. The resulting red precipitate was washed with copious amounts of DI water and dried under vacuum to yield 310 mg (98%) of red powder. ¹H NMR (CDCl₃ with drop of *d*-TFA): 9.91 (d, 2H, *J* = 8.8 Hz), 8.79 (d, 2H, *J* = 8.3 Hz), 8.49 (s, 2H), 7.59 (d, 4H, *J* = 8.8 Hz), 7.19 (d, 4H, *J* = 8.3 Hz), 5.03 (d, 4H, *J* = 2.4 Hz), 2.22 (t, 2H, *J* = 2.4 Hz), 1.41 (s, 18H); HR-ESI MS *m/z* calculated for [M + H]⁺ 763.2803 found [M + H]⁺ 763.2806.

Synthesis of *N,N'*-dipropargyl-(1,7)-di(dodecylthio)perylene-3,4:9,10-bis(dicarboximide) (mixture of 1,6- and 1,7-isomers) (Thiol-PDI). 6 (250 mg, 0.32 mmol), propargylamine (50 mg, 0.91 mmol), 90 μL of glacial acetic acid, 15 mL of anhydrous NMP were added to a reaction flask. The reaction mixture was

stirred at 80 °C under N₂ for 15 hours. The reaction mixture was cooled to room temperature and poured into 50 mL of DI water. The precipitate was washed with copious water and then dried under vacuum. Purification by silica preparatory TLC plates using CHCl₃ as running solvent afforded 180 mg of **6** (66% yield). ¹H NMR (CDCl₃, 1,6-isomer): 8.84 (d, 2H, *J* = 7.8 Hz), 8.82 (d, 2H, *J* = 7.8 Hz), 8.75 (s, 2H), 5.03 (d, 2H, *J* = 2.4), 5.01 (d, 2H, *J* = 2.4), 3.19 (t, 4H, *J* = 7.3 Hz), 2.25 (t, 1H, *J* = 2.4 Hz), 2.21 (t, 1H, *J* = 2.4 Hz), 1.66 (q, 4H, *J* = 7.4 Hz), 1.39 (q, 4H, *J* = 7.4 Hz), 1.3–1.2 (br, 32H), 0.92 (t, 6H, *J* = 7.3 Hz); ¹H NMR (CDCl₃, 1,7-isomer): 8.84 (d, 2H, *J* = 7.8 Hz), 8.80 (s, 2H), 8.71 (d, 2H, *J* = 7.8 Hz), 5.01 (d, 4H, *J* = 1.8 Hz), 3.19 (t, 4H, *J* = 7.3), 2.23 (t, 2H, *J* = 1.8 Hz), 1.68 (q, 4H, *J* = 7.4 Hz), 1.43 (q, 4H, 7.4 Hz), 1.3–1.2 (br, 32H), 0.88 (t, 6H, *J* = 7.3 Hz); HR-ESI MS *m/z* calculated for [M + H]⁺ 867.4224 found [M + H]⁺ 867.4223.

Synthesis of *N,N'*-dipropargyl-(1,7)-dipyrrolidinylperylene-3,4:9,10-bis(dicarboximide) (mixture of 1,6- and 1,7-isomers) (Pyr-PDI). **7** (53.7 mg, 0.10 mmol), propargylamine (70 mg, 1.3 mmol), and 5 mL of dry DMF was added to a reaction flask. The solution was heated to 125 °C under N₂ for two hours. The reaction was removed from heat and allowed to cool and was then poured into 100 mL of cold DI water. The product was filtered and rinsed with copious amounts of DI water. The final product was dried under vacuum to yield 60.1 mg (98%) of green product. ¹H NMR (CDCl₃): 8.53 (s, 2H), 8.49 (d, 2H, *J* = 8.3 Hz), 7.71 (d, 2H, *J* = 8.3 Hz), 5.02 (d, 4H, *J* = 2.4 Hz), 3.76 (br, 4H), 2.84 (br, 4H), 2.20 (t, 2H, *J* = 2.4 Hz), 2.10 (br, 4H), 1.99 (br, 4H); HR-ESI MS *m/z* calculated for [M]⁺ 604.2105 found [M]⁺ 604.2107.

Azido-SAM formation on glass and ITO

Glass slides were washed sequentially with acetone, DCM, MeOH, and DI water prior to exposure to a piranha solution for 30 minutes. (Piranha solution consists of a 3 : 1 v/v concentrated sulfuric acid to 30% hydrogen peroxide, CAUTION! Extremely exothermic and reacts with organics.) ITO coated glass slides were sonicated in a dilute solution of Alconox for ten minutes, washed with the same solvents, and then soaked in concentrated sulfuric acid for 30 minutes to generate a dense population of surface hydroxides. Next, both glass and ITO slides were then rinsed with copious amounts of DI water, dried under a stream of nitrogen, and placed in a Schlenk flask at a pressure of ~10⁻³ Torr to remove residual surface water. Nitrogen was replaced in the flask and a solution of approximately 1 mM 11-azidoundecyltrimethoxysilane in anhydrous toluene were added to the flask and heated to 65–70 °C for 12 hours. After cooling to room temperature, the slides were sonicated in fresh toluene for five minutes, washed sequentially with toluene, acetone, DCM, MeOH, and DI water, and dried with a stream of nitrogen. Finally, the slides were placed in an oven at 75 °C under 10⁻³ Torr and dried overnight.

Multilayer fabrication

Layer additions of **PhO-PDI** and **Pyr-PDI**: a solution of DMF containing ~14% water, 1.2 mM of PDI, 0.9 mM CuSO₄, 1 mM either TBTA or THPTA, and 1.4 mM sodium ascorbate was

placed in contact with one side of a SAM-functionalized slide placed in a covered Petri dish in a 30 °C oven. After ten minutes, the slide was washed with acetone, 95 : 5 mixture of DCM–MeOH, MeOH, 1 mM disodium ethylenediaminetetraacetate in 1 : 1 ethanol : DI water mixture, and DI water.

Layer additions of **Thiol-PDI**: a solution of DMSO containing ~3% water, 1.2 mM of perylene dye, 1.2 mM CuSO₄, 1.3 mM THPTA, and 1.8 mM sodium ascorbate was similarly prepared as above.

Layer additions of **N₃Mest**: a solution of DMSO containing ~14% water, 2.2 mM of **N₃Mest**, 4.4 mM CuSO₄, 4.9 mM TBTA, and 8.9 mM sodium ascorbate was placed in contact with the dye side of the substrate and placed in a covered Petri dish in a 30 °C oven. After ten minutes the slide was washed with the same solvents as above.

Electronic absorption spectroscopy

UV-visible electronic absorption spectra were taken on a Perkin-Elmer Lambda 950 UV/vis Spectrometer with slides held normal to the incident light beam in air. Samples were background subtracted using a SAM functionalized glass or ITO slide. Polarized absorbance spectra were taken with the thin film sample along with a corresponding SAM background positioned at 30, 45 and 90° angles with respect to the incident light. The incident light was polarized using a Glan-Taylor prism.

Infrared spectroscopy

FTIR absorption spectra were measured by a Bio-Rad (Varian) Excalibur FTS 4000 infrared spectrometer using a liquid nitrogen cooled MCT detector and VariGATR attenuated total reflectance accessory (Harrick Scientific) equipped with a single reflection hemispherical Ge crystal. The GATR accessory was continually purged with dried nitrogen in order to maintain a constant atmosphere. A stream of nitrogen gas was passed over the thin film samples and the Ge crystal to remove dust prior to every scan. Samples were pressed against the crystal surface using a high torque slip-clutch pressure applicator to ensure consistent pressure over all scans. The light beam was held at an angle of 60° versus normal with the light polarized perpendicular to the surface using a Wire Grid Polarizer (Harrick Scientific). Scans were acquired with the Varian Resolutions Pro software at a resolution of 4 cm⁻¹ scanned 256 times. The scans were ratioed against a freshly cleaned ITO slide background using a UVO cleaner (UV Ozone Bioforce ProCleaner Plus) for at least 5 minutes. The resulting transmission spectra were converted to absorbance then were baseline corrected using multiple points void of major IR transitions. After baseline correction, the azide stretch at 2100 cm⁻¹ was integrated to determine azide content within the thin films for each layer.

Electrochemistry

Electrochemical measurements were performed using a CH Instruments 440A potentiostat in a three electrode configuration. Multilayer samples on ITO were used as the working electrode and the area defined by a cylindrically bored hole in Teflon cone pressed firmly on the sample. A silver wire was used

a pseudo reference electrode and calibrated with ferrocene after each experiment. A freshly cleaned Pt wire was used as the counter electrode. All electrochemical experiments were performed using 0.1 M TBAP electrolyte in dry acetonitrile under a N₂ environment.

Acknowledgements

We thank Dr Ellen Miseo (Analytical Answers, Inc.) for assistance with IR analysis, Carolyn A. Buckley for assistance in optimizing surface reaction conditions, and Zhaorui Huang for help in the synthesis of **6**. EEB acknowledges a Darrin Foundation fellowship. This material is based upon work supported by the National Science Foundation under CHE-1255100.

Notes and references

- 1 J. H. Alstrum-Acevedo, M. K. Brennaman and T. J. Meyer, *Inorg. Chem.*, 2005, **44**, 6802–6827.
- 2 T. J. Meyer, *Acc. Chem. Res.*, 1989, **22**, 163–170.
- 3 M. H. V. Huynh, D. M. Dattelbaum and T. J. Meyer, *Coord. Chem. Rev.*, 2005, **249**, 457–483.
- 4 D. Holten, D. F. Bocian and J. S. Lindsey, *Acc. Chem. Res.*, 2002, **35**, 57–69.
- 5 M. R. Wasielewski, *Chem. Rev.*, 1992, **92**, 435–461.
- 6 M. R. Wasielewski, *Acc. Chem. Res.*, 2009, **42**, 1910–1921.
- 7 D. Gust, T. A. Moore and A. L. Moore, *Acc. Chem. Res.*, 2001, **34**, 40–48.
- 8 D. Gust, T. A. Moore and A. L. Moore, *Acc. Chem. Res.*, 1993, **26**, 198–205.
- 9 D. Gust, T. A. Moore and A. L. Moore, *Acc. Chem. Res.*, 2009, **42**, 1890–1898.
- 10 L. Netzer and J. Sagiv, *J. Am. Chem. Soc.*, 1983, **105**, 674–676.
- 11 M. Pomerantz, A. Segmueller, L. Netzer and J. Sagiv, *Thin Solid Films*, 1985, **132**, 153–162.
- 12 A. Ulman and N. Tillman, *Langmuir*, 1989, **5**, 1418–1420.
- 13 R. Maoz and J. Sagiv, *Adv. Mater.*, 1998, **10**, 580–584.
- 14 A. Baptiste, A. Gibaud, J. F. Bardeau, K. Wen, R. Maoz, J. Sagiv and B. M. Ocko, *Langmuir*, 2002, **18**, 3916–3922.
- 15 A. Ulman, *Chem. Rev.*, 1996, **96**, 1533–1554.
- 16 D. Li, M. A. Ratner, T. J. Marks, C. Zhang, J. Yang and G. K. Wong, *J. Am. Chem. Soc.*, 1990, **112**, 7389–7390.
- 17 H. Lee, L. J. Kepley, H. G. Hong and T. E. Mallouk, *J. Am. Chem. Soc.*, 1988, **110**, 618–620.
- 18 H.-N. Kim, S. W. Keller, T. E. Mallouk, J. Schmitt and G. Decher, *Chem. Mater.*, 1997, **9**, 1414–1421.
- 19 H. Lee, L. J. Kepley, H. G. Hong, S. Akhter and T. E. Mallouk, *J. Phys. Chem.*, 1988, **92**, 2597–2601.
- 20 H. G. Hong, D. D. Sackett and T. E. Mallouk, *Chem. Mater.*, 1991, **3**, 521–527.
- 21 H. C. Yang, K. Aoki, H. G. Hong, D. D. Sackett, M. F. Arendt, S. L. Yau, C. M. Bell and T. E. Mallouk, *J. Am. Chem. Soc.*, 1993, **115**, 11855–11862.
- 22 P. G. Hoertz and T. E. Mallouk, *Inorg. Chem.*, 2005, **44**, 6828–6840.
- 23 J. Jiao, F. Anariba, H. Tiznado, I. Schmidt, J. S. Lindsey, F. Zaera and D. F. Bocian, *J. Am. Chem. Soc.*, 2006, **128**, 6965–6974.
- 24 M. A. Ansell, E. B. Cogan and C. J. Page, *Langmuir*, 2000, **16**, 1172–1179.
- 25 A. Hatzor, T. Van der Boom-Moav, S. Yochelis, A. Vaskevich, A. Shanzer and I. Rubinstein, *Langmuir*, 2000, **16**, 4420–4423.
- 26 C. Lin and C. R. Kagan, *J. Am. Chem. Soc.*, 2003, **125**, 336–337.
- 27 M. Altman, A. D. Shukla, T. Zubkov, G. Evmenenko, P. Dutta and M. E. vanderBoom, *J. Am. Chem. Soc.*, 2006, **128**, 7374–7382.
- 28 L. Kosbar, C. Srinivasan, A. Afzali, T. Graham, M. Copel and L. Krusin-Elbaum, *Langmuir*, 2006, **22**, 7631–7638.
- 29 M. Maskus and H. D. Abruna, *Langmuir*, 1996, **12**, 4455–4462.
- 30 P. K. B. Palomaki and P. H. Dinolfo, *Langmuir*, 2010, **26**, 9677–9685.
- 31 P. K. B. Palomaki, A. Krawicz and P. H. Dinolfo, *Langmuir*, 2011, **27**, 4613–4622.
- 32 A. Krawicz, J. Palazzo, G.-C. Wang and P. H. Dinolfo, *RSC Adv.*, 2012, **2**, 7513–7522.
- 33 P. K. B. Palomaki and P. H. Dinolfo, *ACS Appl. Mater. Interfaces*, 2011, **3**, 4703–4713.
- 34 P. K. B. Palomaki, M. R. Civic and P. H. Dinolfo, *ACS Appl. Mater. Interfaces*, 2013, **5**, 7604–7612.
- 35 X. Li, L. E. Sinks, B. Rybtchinski and M. R. Wasielewski, *J. Am. Chem. Soc.*, 2004, **126**, 10810–10811.
- 36 A. Marcos Ramos, E. H. A. Beckers, T. Offermans, S. C. J. Meskers and R. A. J. Janssen, *J. Phys. Chem. A*, 2004, **108**, 8201–8211.
- 37 B. Rybtchinski, L. E. Sinks and M. R. Wasielewski, *J. Am. Chem. Soc.*, 2004, **126**, 12268–12269.
- 38 C. Zhao, Y. Zhang, R. Li, X. Li and J. Jiang, *J. Org. Chem.*, 2007, **72**, 2402–2410.
- 39 M. Cotlet, T. Vosch, S. Habuchi, T. Weil, K. Müllen, J. Hofkens and F. De Schryver, *J. Am. Chem. Soc.*, 2005, **127**, 9760–9768.
- 40 C. Huang, S. Barlow and S. R. Marder, *J. Org. Chem.*, 2011, **76**, 2386–2407.
- 41 F. Würthner, V. Stepanenko, Z. Chen, C. R. Saha-Möller, N. Kocher and D. Stalke, *J. Org. Chem.*, 2004, **69**, 7933–7939.
- 42 P. K. B. Palomaki and P. H. Dinolfo, *ACS Appl. Mater. Interfaces*, 2011, **3**, 4703–4713.
- 43 S. Ghosh, X.-Q. Li, V. Stepanenko and F. Würthner, *Chemistry*, 2008, **14**, 11343–11357.
- 44 Z. Chen, V. Stepanenko, V. Dehm, P. Prins, L. D. a. Siebbeles, J. Seibt, P. Marquetand, V. Engel and F. Würthner, *Chemistry*, 2007, **13**, 436–449.
- 45 F. Würthner, C. Bauer, V. Stepanenko and S. Yagai, *Adv. Mater.*, 2008, **20**, 1695–1698.
- 46 F. Würthner, Z. Chen, V. Dehm and V. Stepanenko, *Chem. Commun.*, 2006, 1188–1190.
- 47 Y. Liu, K.-R. Wang, D.-S. Guo and B.-P. Jiang, *Adv. Funct. Mater.*, 2009, **19**, 2230–2235.
- 48 M. J. Fuller, L. E. Sinks, B. Rybtchinski, J. M. Giaimo, X. Li and M. R. Wasielewski, *J. Phys. Chem. A*, 2005, **109**, 970–975.

- 49 S. Yagai, T. Seki, T. Karatsu, A. Kitamura and F. Würthner, *Angew. Chem., Int. Ed. Engl.*, 2008, **47**, 3367–3371.
- 50 Y.-S. Ma, C.-H. Wang, Y.-J. Zhao, Y. Yu, C.-X. Han, X.-J. Qiu and Z. Shi, *Supramol. Chem.*, 2007, **19**, 141–149.
- 51 B. Valeur, *Molecular Fluorescence: Principles and Applications*, WILEY-VCH Verlag GmbH, Weinheim, Germany, 2002.
- 52 Z. Zhang, R. Hu and Z. Liu, *Langmuir*, 2000, **16**, 1158–1162.
- 53 J. K. Blasie, M. Erecińska, S. Samuels and J. S. Leigh, *Biochim. Biophys. Acta, Bioenerg.*, 1978, **501**, 33–52.
- 54 D.-J. Qian, C. Nakamura, T. Ishida, S.-O. Wenk, T. Wakayama, S. Takeda and J. Miyake, *Langmuir*, 2002, **18**, 10237–10242.
- 55 M. Sadrai, L. Hadel, R. R. Sauers, S. Husain, K. Krogh-Jespersen, J. D. Westbrook and G. R. Bird, *J. Phys. Chem.*, 1992, **96**, 7988–7996.
- 56 J. P. Collman, N. K. Devaraj, T. P. A. Eberspacher and C. E. D. Chidsey, *Langmuir*, 2006, **22**, 2457–2464.
- 57 X. Ji, Z. Ge, J. Bu, Q. Liu, W. Wang and C. Xu, *Chin. Chem. Lett.*, 2013, **25**, 292–294.
- 58 M. Milosevic, S. Berets and A. Fadeev, *Appl. Spectrosc.*, 2003, **57**, 724–727.
- 59 Y. Ito, A. a. Virkar, S. Mannsfeld, J. H. Oh, M. Toney, J. Locklin and Z. Bao, *J. Am. Chem. Soc.*, 2009, **131**, 9396–9404.
- 60 A. Łapiński, A. Graja, I. Olejniczak, A. Bogucki, M. Połomska, J. Baffreau, L. Perrin, S. Leroy-Lhez and P. Hudhomme, *Mol. Cryst. Liq. Cryst.*, 2006, **447**, 87/[405]–103/[421].
- 61 B. Liu, M. Shi, L. Yang, H. Chen and M. Wang, *Sci. China, Ser. B: Chem.*, 2008, **51**, 152–157.
- 62 V. P. Tolstoy, I. V. Chernyshova, and V. A. Skryshevsky, *Handbook of Infrared Spectroscopy of Ultrathin Films*, Wiley-Interscience, Hoboken, NJ, 2003.
- 63 R. K. Dubey, M. Niemi, K. Kaunisto, K. Stranius, A. Efimov, N. V. Tkachenko and H. Lemmetyinen, *Inorg. Chem.*, 2013, **52**, 9761–9773.
- 64 A. S. Lukas, Y. Zhao, S. E. Miller and M. R. Wasielewski, *J. Phys. Chem. B*, 2002, **106**, 1299–1306.
- 65 A. J. Bard and L. R. Faulkner, *Electrochemical methods: fundamentals and applications*, Wiley, New York, 2nd edn, 2001.
- 66 Y. Fu and S. J. Yu, *Angew. Chem., Int. Ed.*, 2001, **40**, 437–440.
- 67 Y. Song, E. K. Kohlmeir and T. J. Meade, *J. Am. Chem. Soc.*, 2008, **130**, 6662–6663.
- 68 T. R. Chan, R. Hilgraf, K. B. Sharpless and V. V. Fokin, *Org. Lett.*, 2004, **6**, 2853–2855.
- 69 H. A. Michaels and L. Zhu, *Chem.-Asian J.*, 2011, **6**, 2825–2834.
- 70 P. K. B. Palomaki and P. H. Dinolfo, *Langmuir*, 2010, **26**, 9677–9685.
- 71 A. Böhm, H. Arms, G. Henning and P. Blaschka, *Ger. Pat. Appl.*, 1997, vol. DE 19547209 A1.
- 72 Y. Zhao and M. R. Wasielewski, *Tetrahedron Lett.*, 1999, **40**, 7047–7050.
- 73 T. Ishi-i, K. Murakami, Y. Imai and S. Mataka, *Org. Lett.*, 2005, **7**, 3175–3178.
- 74 L. M. A. Perdigão, A. Saywell, G. N. Fontes, P. A. Staniec, G. Goretzki, A. G. Phillips, N. R. Champness and P. H. Beton, *Chem.-Eur. J.*, 2008, **14**, 7600–7607.